NJC

Accepted Manuscript

This article can be cited before page numbers have been issued, to do this please use: G. Zhao, Y. Zhu, S. Guang, F. Ke and H. Xu, *New J. Chem.*, 2017, DOI: 10.1039/C7NJ03692B.

ROYAL SOCIETY OF CHEMISTRY

rsc.li/njc

View Article Online
DOI: 10.1039/C7NJ03692B

Facile preparation and properties of single molecular POSS-based white-light-emitting hybrid materials by click chemistry

Gang Zhao, [a] Yakun Zhu, [a] Shanyi Guang,[b*] Fuyou Ke, [a] Hongyao Xu [a*]

[a] State Key Laboratory for Modification of Chemical Fibers and Polymer Materials & College of Material Science and Engineering, Donghua University, Shanghai 201620, China

[b] School of Chemistry, Chemical and Bioengineering, Donghua University, Shanghai, 201620, China

College of Material Science and Engineering & State Key Laboratory of Chemical Fibers and Polymeric Materials modification, Donghua University, Shanghai 201620, China.

*Corresponding Author: Professor Hongyao Xu.

Tel: +86-21-67792874, E-mail: hongyaoxu@163.com

ABSTRACT: Recently, Organic white light emitting devices (OWLEDs) have attracted great interest in the flexible displays and solid state lighting devices. Here we report a kind of novel POSS-based white-light-emitting single molecular nanohybrid (POSS-WLED), which was precisely controllably prepared via click chemistry by simple controlling the feed ratio of blue (**B**) and yellow (**Y**) emitting units. It was found that the self-absorption of emitting component and the intramolecular energy transfer was well adjusted based on theoretical simulation and molecular design. The incorporation of nanosized inorganic POSS effectively restrained intramolecular rotation (RIR) and shows significantly decoupling effect of emitter and AIE (aggregation induced enhancement) effect, which provided an important contribution to high emission efficiency of hybrid molecules. The resultant nanometer organic-inorganic hybrid ($\mathbf{W_{62}}$) exhibited significantly enhanced emission in the solid film (Φ_{film}=95%) because of significantly AIE effect which is attributed to the incorporation of nano-sized POSS moiety. Herein, this work will provide a novel strategy for design and preparation of highly efficiency white-light-emitting molecules with high emission efficiency, thermal stability, and well film formability.

1. Introduction

View Article Online
DOI: 10.1039/C7NJ03692B

Nowadays, single molecular organic white light emitting materials, as a novel type luminescent medium, have become increasingly popular in contemporary research owing to their potential for applications in flexible displays and solid state lighting sources [1-8]. Compared with multicomponent molecular emitters of white-light-emitting devices (WLEDs), single molecular organic white light emitters have exhibited some prominent advantages such as perfect color reproducibility and stability [9-17]. In the previous literatures, white-light-emitting single molecules are mainly focused on polymers, which are composed of covalently linked different emitter components on the backbone or in side groups. The white light emissions in these polymers are generated via utilizing partial energy transfer from a wider band-gap donor component to a narrower band-gap acceptor [18-22]. However, the inherent poor purity, low multi-polydispersity, and low thermal properties of polymers have greatly limited their luminous efficiency and practical application. Hence, design and preparation of the organic white-light-emitting macromolecule with high thermal properties and well luminous efficiency will be a key issue for their application in the flexible display. However, the inevitable energy transfer makes the molecular design difficult. As the best knowledge of us, only Park and his coworkers [23,24] reported an excited-state intramolecular proton transfer molecule composed of covalently linked blue- and orange-light-emitting moieties, which energy transfer was entirely frustrated and white luminescence was achieved. However, small organic molecules often exhibited low thermal properties.

Accordingly, it is a challenge to seek an alternation material system that combines the benefits of organic small molecules (e.g., high purity), inorganic moiety (high thermal stability) and polymers (e.g., good film forming ability and low processing cost). The discovery of polyhedral oligomeric silsesquoixanes (POSS) with special structure provided an important chance to solve these problems. POSS is a nanometer-sized cube-like molecule with inorganic core surrounded by eight organic corner groups (active or inert), which has been demonstrated to be an excellent platform and building block for architecture of novel 3D organic-inorganic molecular hybrid materials with a number of desirable properties [25-31]. Rigid POSS cage enables them to significantly improve the thermal and mechanical properties of the materials. In our previous work, many POSSs containing organic-inorganic molecular hybrids were designed and prepared for investigation of preparation methods of these hybrids and enhancement mechanisms of their thermal properties [29-31,32-33]. Moreover, some functional hybrids with high thermal stability and nonlinear optical properties were

View Article Online
DOI: 10.1039/C7NJ03692B

prepared and the enhancement mechanisms of optical properties were investigated [34,41,42]. It was found that a suitable molecular design will effectively improve the thermal stability and optical properties.

In this paper, based on theoretical simulation, three POSS-based luminous single molecular nanohybrids containing a yellow monochromatic emitter (**Y**) with a large Stokes shift and a blue monochromatic emitter (**B**) were designed and prepared, where both emitters possess similar absorption spectra to avoid the strong self-absorption between different emitter. The partial energy transfer from **B** to **Y** is allowed for effectively adjusting the balance of the white light emission. It is hopefully realized that the incorporation of nanosized inorganic POSS can inhibit molecular aggregation and improve the luminous efficiency. In addition, emission mechanism of white light of single nanohybrid molecule was also investigated in detail on the basis of experimental and theoretical method.

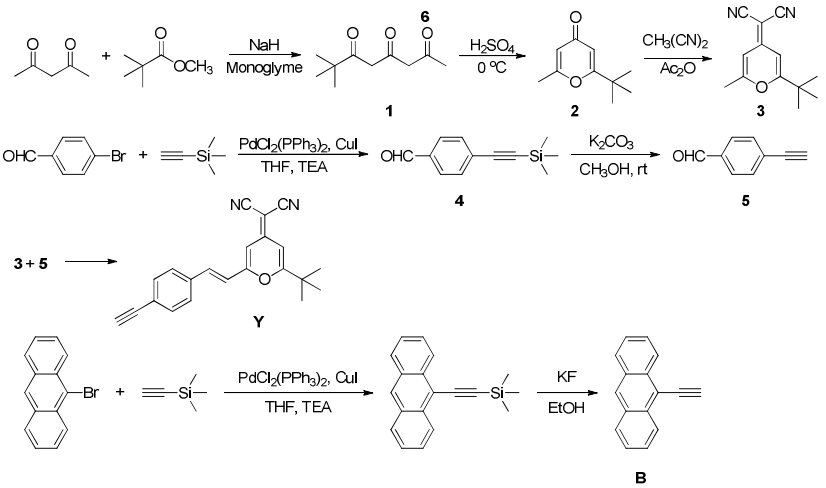

Scheme 1. The synthetic route of the blue monomer (**B**) and the yellow monomer (**Y**).

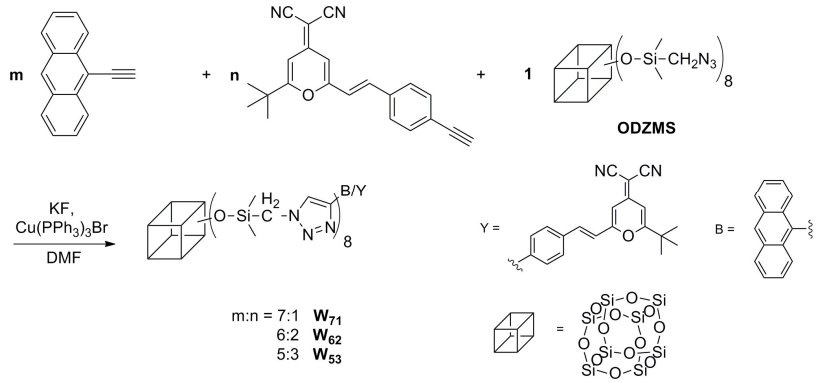

Scheme 2. The synthetic route of white-light hybrids.

View Article Online
DOI: 10.1039/C7NJ03692B

2. Experimental

2.1. Materials

Unless otherwise noted, all commercial reagents were used as received. $PdCl_2(PPh_3)_2$, 9-bromoanthracene, 1,2-dimethoxyethaneand ethynyltrimethylsilane were purchased from J&K Scientific LTD. NaN_3, 4-bromobenzaldehyde and CuI were purchased from Shanghai Jiachen Chemical Plant. Acetylacetone, NaOH, tetrabutylammonium bromide, DMSO, 1, 4-dioxane, KF, CuBr, PPh_3 and THF were purchased from Shanghai Chemical Reagent Company. Octakis(azidomethyl)(dimethylsiloxy)octasilsequioxane (ODZMS) were obtained according to the literature procedure [35]. The TEA and THF solution was distilled immediately prior to use.

2.2. Instruments

FTIR spectra were recorded as KBr disk by a Nicolet NEXUS 8700 FTIR spectrometer. ^{1}H NMR spectra were collected on a Bruker DMX-400 spectrometer using chloroform ($CDCl_3$) as solvent. ^{29}Si NMR measurements were obtained at room temperature using a Bruker DMX-400 spectrometer at a resonance frequency of 79.49 MHz. Matrix assisted laser desorption ionization time of flight mass spectrometry (MALDI-TOF MS) was carried out using a Voyager-DE RP in linear and reflection modes. The optical properties of the samples were measured by Shimadzu UV-265 spectrophotometer and FP6600 Fluorescence spectrometer with a 1 cm quartz cell in tetrahydrofuran (THF, 1×10^{-5} M). Elemental analysis (EA) was carried out by a CHNOS Elemental Analyzer, vario EI Ⅲ. DSC (differential scanning calorimetry) was performed on a TA instruments DSC 9000 equiped with a liquid nitrogen cooling accessory unit under a continuous purge (50 mL min^{-1}). The scan rate was carried out at a heating of 10 ^{o}C min^{-1} within the temperature range 20-300 ^{o}C thermogravimetric analysis (TGA) were obtained by a Perkin-Elmer TGA under an nitrogen atmosphere at a heating rate of 10 ^{o}C min^{-1}. The atomic force microscope (AFM) images of films were obtained by trapping mode on Agilent 5500 AFM.

Quantum Efficiency: Photoluminescence excitation (PLE) was defined through a modification of relative approach to describe via Crosby and Demas using 1,10-diphenylanthracence as references. The absorption at 365 nm was established for each materials at different concentrations (maximum absorption of 20%). Then these samples were diluted through equal number so as to prevent excimer formation and fluorimeter saturation, and the whole area of the emission spectrum was calculated.

View Article Online
DOI: 10.1039/C7NJ03692B

For each solvent, absorption and emission measurements were duplicated at least two times and averaged. The slop of a plot of emission versus absorption was ascertained for each materials, and according to the equation $\Phi_{PL(x)}=(A_s/A_x)(F_x/F_s)(n_x/n_s)^2\Phi_{PL(x)}$ was calculated the relative quantum efficiency.

Where *x* is the sample to evaluated, s the reference, *A* the absorption at the excitation wavelength, *F* the entire integrated emission, *n* the refraction index of the solvent, and the quantum Φ_{PL} yield. The materials of PLQE (Φ) in film was collected through 9,10-diphenylanthrancene (scattered in the PMMA film with a concentration lower than 1×10^{-3} M and a PLQE of 83%) as a standard.

2.3. Synthesis

The synthesis of the monomers and hybrid materials is shown in Scheme 1 and Scheme 2, respectively. The experimental details are described as follows:

*2.3.1. Synthesis of 2-methyl-6-tertbutyl-4H-pyrone (**2**).*

The compound **2** was obtained according to the literature procedure [36]. The isolated yield of the product was 80 %. ^{1}H NMR (400 MHz, 298 K, $CDCl_3$): δ = 6.16 (s, 1H, *J*=2.17 Hz, Pr-H), 6.07 (s, 1H, Pr-H), 2.43 (s, 3H, CH_3), 1.35 (s, 9H, $C(CH_3)_3$). FTIR (KBr), *v* (cm^{-1}): 3070 (w, C=C-H), 2972, 2932, 2871 (m, -CH), 1655 (s, C=O).

*2.3.2. Synthesis of 2-(2-tertbutyl-6-methyl-4H-4-pyranyl) malononitrile **(3)**.*

The compound **3** was prepared by between compound 2 and malononitrile according to literature procedure [36]. ^{1}H NMR (400 MHz, 298 K, $CDCl_3$): δ = 6.49-6.50 (m, 2H, Pr-H), 2.27 (s, 3H, CH_3), 1.23 (s, 9H, $C(CH_3)_3$). FTIR (KBr), *v* (cm^{-1}): 2970, 2879 (m, -CH_3), 2212 (s, -CN), 1652 (C=C), 1342, 1275, 1201 (m, C-O-C).

*2.3.3. Synthesis of 4-trimethylsilyl ethynylbenzaldehyde **(4)**.*

The compound **3** was also prepared based on the reported literature in prior [37]. Yield: 85%. ^{1}H NMR (400 MHz, 298 K, $CDCl_3$): δ = 9.93 (s, 1H, CHO), 7.74-7.76 (d, 2H, *J*=8.3 Hz, Ar-H), 7.52-7.55 (d, 2H, *J*=8.3 Hz, Ar-H), 0.20 (s, 9H, CH_3). FTIR (KBr), *v* (cm^{-1}): 2961 (Si-CH), 2830, 2732 (HC=O), 2159 (C≡C), 1705 (C=C), 1251, 845 (Si-C).

*2.3.4. Synthesis of 4-ethynylbenzaldehyde **(5)**.*

Compound **5** was synthesized using a modified literature procedure [38]. Yield 80%. ^{1}H NMR (400 MHz, 298 K, $CDCl_3$): δ =9.95 (s, 1H, H^4), 7.77-7.79 (d, 2H, *J*=8.2Hz, H^4), 7.56-7.58 (d, 2H,

View Article Online
DOI: 10.1039/C7NJ03692B

J=8.2Hz, H^3), 3.23 (s, 1H, H^1). FTIR (KBr, cm^{-1}): 3293 (s, C≡CH), 2107 (C≡C), 1666 (HC=O).

2.3.5. Synthesis of 2-(2-tert butyl-6-(4-alkynyl styrene)-4H-4-sub pyranyl) two propylene nitrile ***(Y)***.

(1.07 g, 5 mmol) **3**, (0.68 g 5.2 mmol) **5** and 0.2 mL pyridine was dissolved in the anhydrous 50 mL acetonitrile and refluxed for 24 h. After cooling the room temperature, **Y** of the resultant precipitation was filtered and rinsed with enough acetonitrile. The crude was recrystallizated by using the mixture solution of THF and ethanol give to yellow crystal **Y** in yield 70%. ^{1}H NMR (400 MHz, 298 K, $CDCl_3$): δ = 7.43-7.49 (m, 5H, H^{2-6}), 7.28-7.32 (d, 1H, H^7), 6.64-6.64 (m, 2H, $H^{8,9}$), 3.23 (s, 1H, H^1), 1.31 (s, 1H, H^{10}). FTIR (KBr), *v* (cm^{-1}): 3243 (s, C≡CH), 2970, 2926, 2855 (w, CH_3), 2103 (C≡C), 1650 (HC=O), 1508 (C=C). ^{13}C NMR (100 MHz, 298 K, $CDCl_3$): δ =32.54, 35.51, 70.12, 81.43, 42.38, 90.83, 112.54, 115.58, 116.63, 121.97, 127.74, 132.26, 134.41, 164.57, 178.43. MALDI-TOF MS $[C_{22}H_{18}N_2O+2H]^+$: Calcd $(M+2H)^+$/z, 326.1403; found M/z), 326.1675

2.3.6. Synthesis of 9-trimethylsilylacetylene anthracene ***(6)***.

Compound 6 was prepared in analogy to a literature procedure [39]. Yield 85%. ^{1}H NMR (400 MHz, 298 K, $CDCl_3$): δ = 8.94-9.01 (m, 3H, $H^{1,5}$), 8.51-8.53 (d, 2H, *J*=8.3Hz, H^2), 8.00-8.14 (m, 4H, $H^{3,4}$), 0.20 (s, 9H, H^6). FTIR (KBr), *v* (cm^{-1}): 3047 (m, Ar-H), 2956 (m; -CH_3), 2144 (w, C≡C), 1623, 884 (m, Ar), 1259, 843, 728 (s, Si $(CH_3)_3$).

2.3.7. Synthesis of 9-ethynyl anthracene ***(B)***.

Compound B was obtained using a modified literature procedure [39]. Yield 78%. ^{1}H NMR (400 MHz, 298 K, $CDCl_3$): δ = 8.44-8.59 (m, 4H, $H^{2,5}$), 7.99-8.03 (m, 1H, H^6), 7.46-7.63 (m, 4H, $H^{3,4}$), 3.99 (s, 1H, H^1). FTIR (KBr), *v* (cm^{-1}): 3261 (s, C≡CH), 3049 (m, ArH), 2956 (m, -CH_3), 2089 (w, C≡C), 1620, 884 (m, Ar).

2.3.8. Preparation of ***(W_{71})***.

To a 100 mL round bottom flask equipped with a magnetic stir bar was added into **6** (0.19g 0.7 mmol), **Y** (0.03g, 0.1 mmol), ODZMS (0.15g, 0.1 mmol), KF (0.23mg 4 mmol), and $Cu(PPh_3)_3Br$ (0.01g, 0.08 mmol) in DMF (50 mL), which refluxed at 110 ^{o}C for 24 h. The reaction mixture was poured into a saturated solution of EDTA and the product was obtained by filtration. The crude product was purified by column chromatography on silica gel (eluent: dichloromethane) to afford fuchsia crystal $\mathbf{W_{71}}$.The isolated yield of the product was 95%. ^{1}H NMR (400 MHz, 298 K, $CDCl_3$): δ = 8.54 (s, 7H, H), 8.19 (s, 8H, H), 8.06 (m, 28H, H), 7.16-7.46 (m, 32H, H), 6.46 (s, 2H, H), 5.29

View Article Online
DOI: 10.1039/C7NJ03692B

(s, 1H, H), 5.15 (S, 1H, H), 1.33 (m, 16H, H), 0.78-0.81(m, 9H, H), 0.01-0.02 (m, 48H, H). ^{29}Si NMR (400 MHz, solid, δ): -65.3 (Ar-CH_2–Si), -79.8 (anthracene-CH_2–Si). FTIR (KBr), ν (cm^{-1}): 3054 (w, Ar-H), 2962, 2929, 2857 (m, -CH_3), 1630 (m, trizole), 1095 (s, Si-O-Si). MALDI-TOF MS $[C_{158}H_{152}N_{26}O_{21}Si_{16}+2H]^+$: Calcd $(M+2H)^+/z$, 3196.7950; found M/z), 3196.7860. Anal. Calcd for $C_{158}H_{152}N_{26}O_{21}Si_{16}$: C, 59.29; H, 4.79; N, 11.38. Found: C, 60.03; H, 4.737; N, 11.13.

2.3.9. Preparation of ***(W_{62})***.

This was prepared as above for $\mathbf{W_{62}}$. The product was yellow powder, yield 97%. ^{1}H NMR (400 MHz, 298 K, $CDCl_3$): δ = 8.54 (s, 7H, H), 8.05-8.07 (m, 6H, H), 8.13-8.15 (s, 8H, H), 8.05-8.07 (m, 24H, H), 7.38-7.49 (m, 32H, H), 6.46 (s, 4H, H), 5.29 (S, 2H, H), 5.15 (S, 2H, H), 1.33 (m, 16H, H), 0.54-0.56 (m, 18H, H), 0.01-0.02 (m, 48H, H). ^{29}Si NMR (400 MHz, solid, δ): -64.8 (Ar-CH_2–Si), -79.1 (anthracene-CH_2-Si). FTIR (KBr), ν (cm^{-1}): 3053 (w; Ar-H), 2964, 2928, 2857 (m, -CH_3), 1650 (m, trizole), 1093 (s, Si-O-Si). MALDI-TOF MS $[C_{164}H_{160}N_{28}O_{22}Si_{16}+2H]^+$: Calcd $(M+2H)^+/z$, 3320.8601; found M/z, 3320.8590. Anal. Calcd for $C_{164}H_{160}N_{28}O_{22}Si_{16}$: C, 59.25; H, 4.85; N, 11.80. Found: C, 59.03; H, 4.658; N, 12.04.

2.3.10. Preparation of ***(W_{53})***.

This was prepared as above for $\mathbf{W_{53}}$. The product was purple powder, yield 92%.^{1}H NMR (400 MHz, 298 K, $CDCl_3$): δ =8.54 (m, 5H, H), 8.12-8.19 (m, 8H, H), 8.06 (m, 20H, H), 7.44-7.58 (m, 32H, H), 6.46 (s, 6H, H), 5.29 (S, 3H, H), 5.15 (S, 3H, H), 1.33 (m, 16H, H), 0.78-0.83 (m, 27H, H), 0.01-0.02 (m, 48H, H). ^{29}Si NMR (400 MHz, solid, δ): -64.6 (Ar-CH_2–Si), -80.5 (anthracene-CH_2–Si). FTIR (KBr), ν (cm^{-1}): 3052(w; ArH), 2963, 2927, 2859 (m, -CH_3), 1635 (m, trizole), 1099 (s, Si-O-Si). MALDI-TOF MS $[C_{170}H_{168}N_{30}O_{23}Si_{16}+H]^+$: Calcd $(M+H)^+/z$, 3444.9257; found 3444.9190. Anal. Calcd for $C_{170}H_{168}N_{30}O_{23}Si_{16}$: C, 59.21; H, 4.91; N, 12.18. Found: C, 58.73; H, 5.031; N, 11.97.

3. Results and discussion

3.1. Theoretical calculation

To validate rationality of structural design of chromophores, a theoretical calculation was conducted using the Gaussian09 software suite with a TD-DFT/6-31G+ level of theory, which was used to simulate the absorption and emission spectra of candidates **B** and **Y** in THF[40,41]. The calculation results are shown in Figure 1. Here, chromophore **B** and **Y** with similar absorption

View Article Online
DOI: 10.1039/C7NJ03692B

spectra and different stokes shift in their emission spectra were selected. It can be concluded from Figure 1, **B** and **Y** show similar absorption spectra, so the same excited light source can be used. Meanwhile, the emission spectrum of **Y** displays very large stokes shift. This not only make emission spectra of **B** and **Y** cover the whole visible range of white light, but inhibits the intramolecular self-absorption. Based on the high efficient "Click chemistry" and covalently incorporation of nano-sized inorganic POSS, the novel hybrid white emission materials with high efficiency is successfully achieved by precisely adjusting the component of **B** and **Y** component.

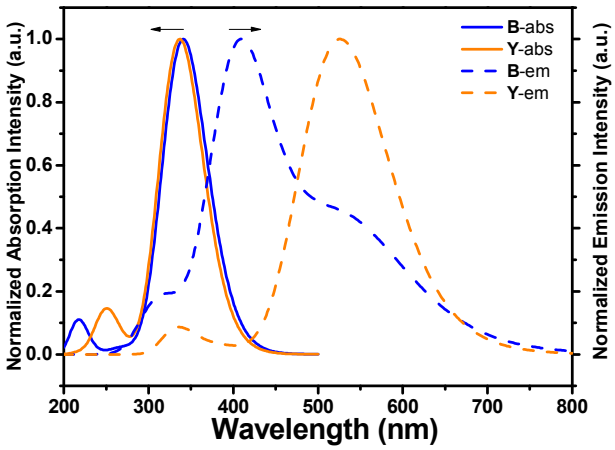

Figure 1. The normalized calculated absorption and emission spectra of **B** and **Y** in THF.

3.2. Synthesis and Characterization

Single molecule organic white light emitters (SMOLEDS) have exhibited some excellent advantages such as perfect color reproducibility, stability and easy fabrication. SMOLEDS mainly concentrated on a series of polymers. However, the inherent poor purity, multi-polydispersity and low thermal properties of polymers have greatly limited their luminous efficiency and practical application. Hence, design and preparation of the hybrid white-light-emitting macromolecule with high thermal properties and well luminous efficiency will be a key issue for their application in the flexible display. Based on the calculation of the density theory, three POSS-based luminous single molecular nanohybrid $\mathbf{W}_{71}$, $\mathbf{W}_{62}$ and $\mathbf{W}_{53}$ containing a yellow monochromatic emitter (**Y**) with a large Stokes shift and a blue monochromatic emitter (**B**), in which the front value in the subscript is defined as number of **B** group, the latter value is the number of **Y** group, were designed and prepared.

View Article Online
DOI: 10.1039/C7NJ03692B

Y and **B** were synthesized by Knovenagel condensation and Sonogashira reaction (supporting information). At first, 4-ethynylbenzaldehyde, a reactant of **Y**, was synthesized from 2-methyl-3-butyn-2-ol. However, intramolecular and intermolecular aldol condensation happened during the hydrolysis reaction and the ideal compound was not obtained. Fortunately, after changing 2-methyl-3-butyn-2-ol to trimethylsilylacetylene, the problem was solved and 4-ethynylbenzaldehyde was prepared successfully. 2-(2-tert-Butyl-6-methylpyran-4-ylidene) malononitrile was prepared following by reference [32]. All purified products gave the characteristic spectroscopic data of FTIR, ^{1}H NMR (see supporting information for details) and elemental analysis corresponding to their expected structures.

In the synthetic process of hybrids, one-step synthesis strategy was employed by highly efficient click chemistry methods. The purification is easily achieved by simply dissolving the precipitation process. Similar one-step strategies were reported in literature [33].

The structure of hybrids $\mathbf{W_{71}}$, $\mathbf{W_{62}}$ and $\mathbf{W_{53}}$ were determined by means of standard spectral methods, elemental analysis and mass spectrum. Figure 2a shows the FTIR spectra of $\mathbf{W_{71}}$, $\mathbf{W_{62}}$ and $\mathbf{W_{53}}$. As shown in Figure 2a, the characteristic absorptions at ~3100, 1625cm^{-1} responding to triazole stretching vibration absorption and the characteristic Si-O-Si stretching vibration of POSS core at ~1100 cm^{-1} appear in spectra of the resulting hybrids, and the characteristic absorptions of –N_3 and C≡C at ~2100 cm^{-1} disappear, indicating that all the eight azide groups of POSS-N_3 completely reacted with alkynyl groups of **B** and **Y** to form the resultant hybrids at almost stoichiometric pattern. In ^{1}H NMR spectra (Figure 2b), it is also found that the characteristic alkyne proton absorption located at 3.13 ppm in the spectrum of **B** and **Y** completely disappears after click reactions and new vibration bands at 1.33 ppm (-SiCH_2) and 0.29 ppm (-SiCH_3) turn up in the ^{1}H NMR spectrum of **ODZMS**, further supporting that objective molecule has been obtained. The characteristic spectral peaks at ~8.54 ppm, assigned to the H proton of triazole, were observed in the spectrum of the resultant hybrids, which further confirm that the click reactions were successfully made. Moreover, the results from C, H, N elemental analyses almost completely corresponding to the theoretical calculated values of objective compounds, further supporting that objective molecules were obtained.

View Article Online
DOI: 10.1039/C7NJ03692B

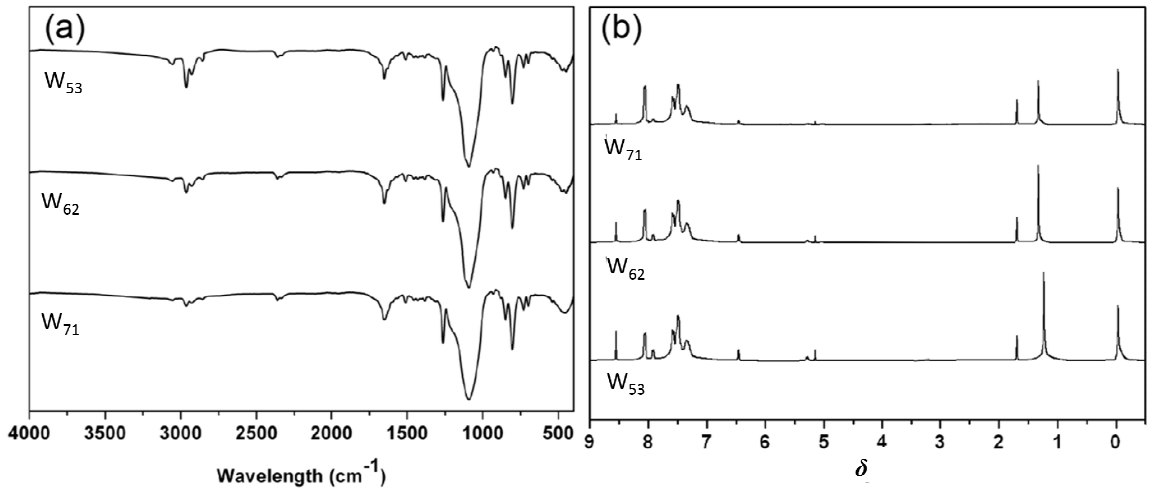

Figure 2. The FTIR and ^{1}H NMR spectra of **W$_{71}$**, **W$_{62}$** and **W$_{53}$**.

3.3. Photophysical Properties

All the resultants molecules **W$_{71}$**, **W$_{62}$** and **W$_{53}$** are soluble in common organic solvents, such as dichloromethane (DCM), tetrahydrofuran (THF), dimethyl sulfoxide (DMSO), *etc*. The solution -based emission and absorption measurements were performed at very low concentrations (10^{-5} M) in an inter-mediate dielectric constant solvent (THF, ε=7.6) to remove the effect of molecular aggregation and differences in molecular dipole moments [53]. The results shown that **Y**'s TLC plate showed a dark point at first, and then exhibited a yellow light point. This may be due to the restriction of intramolecular rotation (RIR) induced emission. Accordingly, the emission spectra of **Y** in THF/water mixture solvent were tested (Figure 3), where THF is a very good solvent and water is a poor solvent. It is found that, in good solvent THF, **Y** shows a weak emission at ~470 nm; but after the addition of poor solvent H_2O (>40% v/v), **Y** exhibits a strong yellow light emission with *ca*. 15 folds enhancement and two the red shift enhanced emission peaks at ~530 nm and 570 nm [28,35,53]. Interestingly, at low water content, the emitting spectrum shows significantly blue shift, then, demonstrated shows a red shift with increase of water content owing to the aggregation enhanced emitting effect. Simultaneously, the emitting intensity enhanced with increase of water content (20 fold at 90 (v/v)% water content) while **Y**'s Stokes shift don't further change after water content more than 40 (v/v)%. As shown in Figure 3a, it emits a bright yellow light in the solid state under 365 nm UV light. These results further indicated that a yellow emitter with large Stokes shift was obtained successfully. Moreover, different from **Y**, the emission spectra of **B** was quickly quenched after the

View Article Online
DOI: 10.1039/C7NJ03692B

poor solvent was added and it fainted in the solid state. These shifts may be in virtue of the dipole-dipole intramolecular interactions between organic moieties and POSS cages to enlarge the torsion angle between the fluorine ring and the triazole ring and low the effective conjugation length of the molecules. Simultaneously, the W_{62}, W_{53}, W_{71} show higher quantum yield of 95%, 83%, 81%, respectively, which are higher than 70% of **B** and 75% of **Y**.

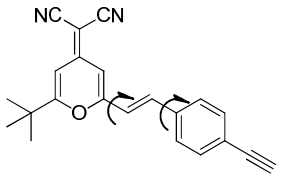

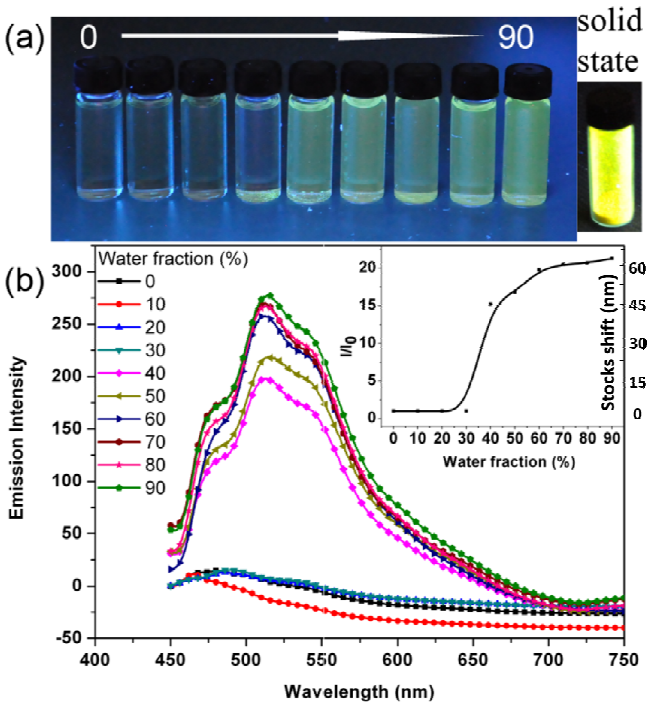

Figure 3. The images of **Y** in THF/Water mixture solvent and solid state (a) and emission spectra of **Y** in THF/Water mixture solvent (b) (10^{-5} mol L^{-1}, λex=365 nm). Inset: changes in the PL peak intensities (*I*) and Stocks shift (nm) of corresponding molecules with different water fractions in the THF/H_2O mixtures.

To evaluate the rationality of our design strategy, the absorption and emission spectra of monochromatic emitters **B** and **Y** in THF and THF/H_2O mixture solvent was compared. Figure 4 is the normalized absorption and emission spectra of **B** and **Y**. As shown in Figure 4, **B** exhibits a

View Article Online
DOI: 10.1039/C7NJ03692B

strong absorption band from 315 to 475 nm, and **Y** shows a boarder absorption bond from 295 to 475 nm. They have an overlap between their absorption spectra at UV bands, which make sure that they can be excited at the same band light, such as 365 nm light from normal UV laps. Meanwhile, the absorption spectrum of **Y** and the emission spectrum of **B** weakly overlap between 390 ~ 475 nm, which effectively limit the intramolecular self-absorption of the resultant hybrids. In addition, the emission spectrum of **B** and **Y** fully cover light band from 400 to 700 nm, which make the realization of white light emission possible.

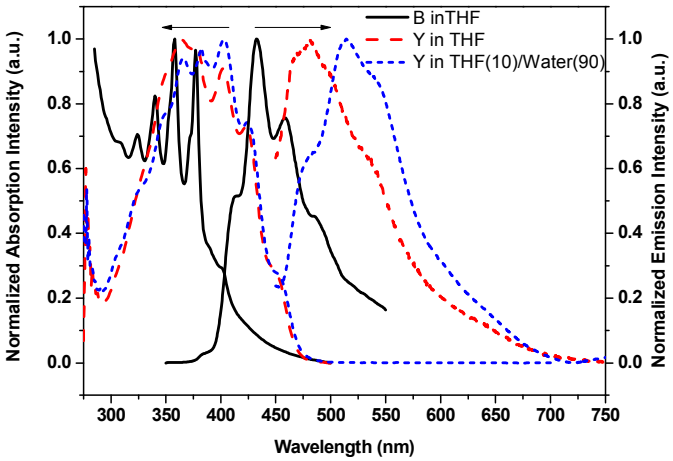

Figure 4. The absorption and emission spectra of **B** and **Y** in THF and **Y** in THF/water (v/v=10: 90) mixture solvent (10^{-5} mol L^{-1}, λex=365 nm).

To further investigate the intramolecular self-absorption of the resultant hybrids, the emission spectra of three hybrids in THF were measured. In good solvent (THF), the emission of **Y** unit is not strong enough to influence the emission spectrum of **B** unit, and change of emission spectra of hybrids can be attributed to the intramolecular self-absorption from **B** to **Y**. As shown in Figure 5, the emission spectrum of $\mathbf{W_{71}}$ shows three peaks at 385, 403 and 431 nm, respectively. With increase of the ratio of yellow unit in hybrids, the emission spectra of the resultant hybrids such as $\mathbf{W_{62}}$ and $\mathbf{W_{53}}$ exhibit two peaks at 410 and 440 nm, respectively. The short wave band UV emission peak at 385 nm disappeared due to intramolecular self-absorption, while the long blue wave band is well kept. These results reveal that the adjusted intramolecular self-absorption occurs in the resultant hybrids: in one hand, the intramolecular self-absorption at blue band was prohibited and the blue

View Article Online
DOI: 10.1039/C7NJ03692B

light-emitting component was well protected; on other hand, the UV-band emission of **B** was self-absorbed by **Y**, which enhance the yellow light-emitting component and further ensure the equilibrious white light emission.

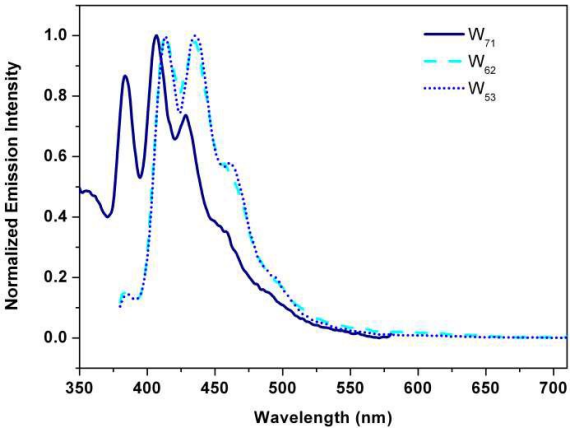

Figure 5. The emission spectra of $\mathbf{W_{71}}$, $\mathbf{W_{62}}$ and $\mathbf{W_{53}}$ in THF (10^{-5} mol L^{-1}, λex=365 nm).

However, in mixed solvent, these resultant hybrids show a quite different spectral characteristics compared to their emission spectra in good solvent THF (Figure 6). After the introduction of POSS, the emission of hybrids with blue band does not quench with the increase of water content due to the disaggregation effect of POSS cage. On the contrary, the emitting intensity shows a little increase, implying that the POSS cage does not prohibit the interactions between **Y** groups and solvent molecules, and the hybrids show an enhanced yellow band emission with the increase of water content owing to the solvent effect. After adjustment of the ratio of **B** and **Y** in hybrids, $\mathbf{W_{71}}$ in the film shows light-blue due to the relatively weak yellow light, whereas $\mathbf{W_{53}}$ exhibits light-green emission due to the relatively strong yellow light (Figure S 22 and Figure S 23). We successfully achieved white light emission from $\mathbf{W_{62}}$ (Figure 6) in THF/Water (10:90 v/v) and film (Figure 7). And its Commission International d'Eclairage (CIE) coordinates is (0.29, 0.34) belonging to white light range.

View Article Online
DOI: 10.1039/C7NJ03692B

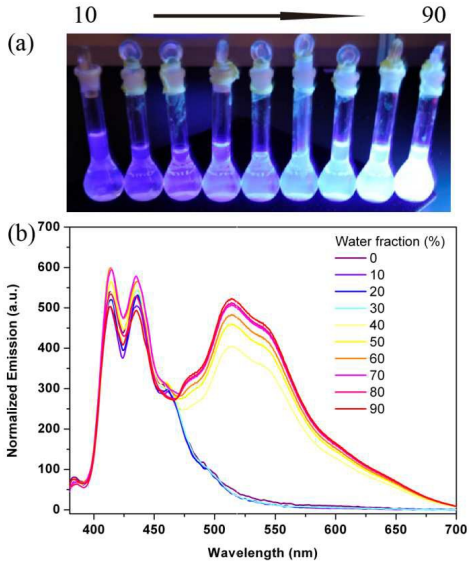

Figure 6. The images (a) and emission spectra (b) of $\mathbf{W_{62}}$ in THF/water mixture solvent (10^{-5} mol L^{-1}, λex=365 nm).

Figure 7 shows the emission properties of $\mathbf{W_{62}}$ in solid state. The film of $\mathbf{W_{62}}$ was prepared by spin-coating the hybrid solutions (*ca*. 10 mg/mL) on quartz plates at 1000 rpm for 30 s. To ensure the accuracy of measurement, three samples were all prepared at the same condition. The AFM image of $\mathbf{W_{62}}$ film show that its surface is quite smooth and no cracks and aggregation are observed (Figure 7a), implying that the resultant organic hybrid has good film formability and structural homogeneity. And the emission spectrum of $\mathbf{W_{62}}$ film was shown in Figure 7c. As shown in Figure 7c, the emission spectrum of $\mathbf{W_{62}}$ film is similar to the emission spectrum of $\mathbf{W_{62}}$ in poor solvent and exhibits a white-light emission over the whole visible range from 400 to 700 nm (Figure 7b, c).

View Article Online
DOI: 10.1039/C7NJ03692B

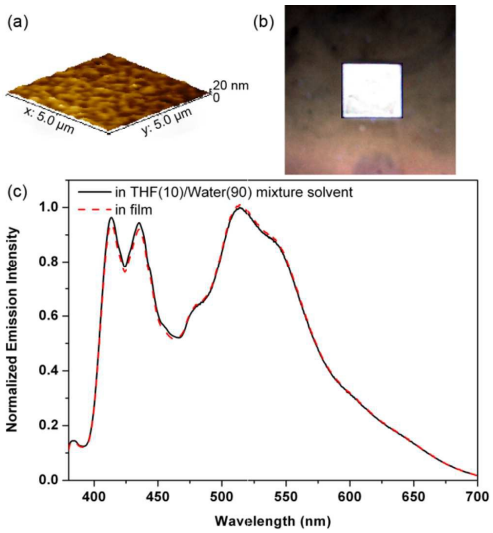

Figure 7. (a) Atomic force microscope images of 5×5 μm^2 tapping mode for $\mathbf{W_{62}}$ film; (b) the images of $\mathbf{W_{62}}$ film under 365 nm UV; (c) the emission spectra of $\mathbf{W_{62}}$ in film and THF/Water (v/v=10:90) mixture solvent (λex=365 nm).

3.4 Thermal Properties

The thermal properties of white light emitting hybrid $\mathbf{W_{62}}$ were measured by TGA and DSC (Figure 8). Usually, the thermal decomposition behavior of POSS macromeres exhibit two step decompositions: the decomposition of organic component and inorganic POSS cage. However, the TGA curve of $\mathbf{W_{62}}$ only shows the one-step decomposition. Meanwhile, $T_{d5\%}$ value of $\mathbf{W_{62}}$ is at *ca.* 273 ^{o}C, which is much higher than 192 ^{o}C of **Y** and 205 ^{o}C of **B** (Figure 8a). Moreover, the char yield of the thermally cured POSSAF was 37.4%, which is not only much higher than that of **B** and **Y** (almost no residual), but also higher than its theoretical rate of residual (28.9%). The thermal stability enhancement and one-step decomposition behaviors are attributed to the uniform incorporation of POSS cage and the jacket effect of the chromophore pendants [35,44-48]: that is, in which the POSS core may have been surrounded by a rigid jacket formed through the strong intra- and inter- molecular electronic interactions of the organic arms, shielding the molecules from the thermal attack. Simultaneously, the triazole ring also enhances the thermal stability of the hybrid nanocomposite. Furthermore, as organic is oxidized away from the surface, the remaining residue becomes enriched in silica and provides a barrier to further oxidation [36,49-52]. Especially, the DSC curves of **B** and **Y** both show a large melting point at ~85 ^{o}C, and Y exhibits a crystallization

View Article Online
DOI: 10.1039/C7NJ03692B

peak at ~ 120 °C. However, the DSC curve of **W_{62}** is quite smooth and there is no melting or crystallization point found (Figure 8b). These results all reveal that the material has excellent amorphous state high thermal stability of **W_{62}** [53].

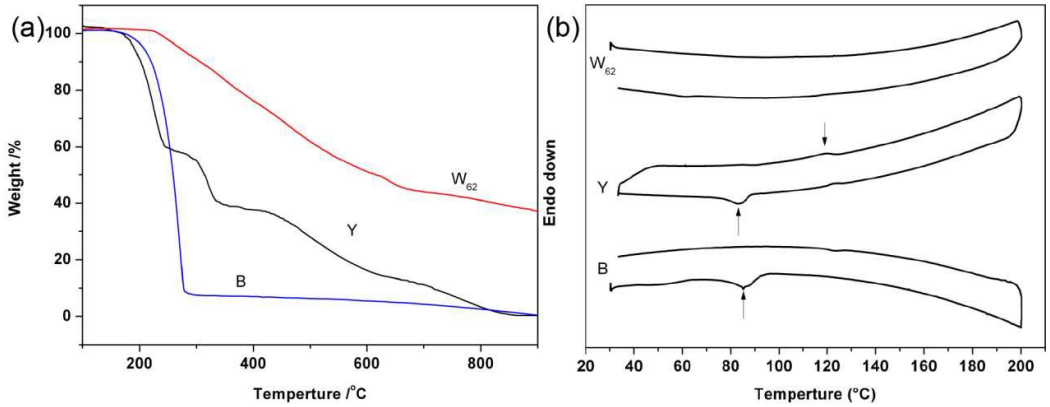

Figure 8. The (a) TGA and (b) DSC curves of **B**, **Y** and **W_{62}**.

4. Conclusions

In conclusions, the novel nano-sized hybrid with white light emission were realized by simple control of the feed ratio of blue and yellow monochromatic moiety in hybrids *via* high efficient "Click chemistry". Based on the theory simulation and molecular design, the optimized molecular structure and composition were obtained (component ratio of **B**: **Y** at 6:2). The investigation of emitting mechanism shows that the allowable transfer in UV band improves the yellow light emission intensity and the restraint of energy transfer in blue band ensures the blue light emission intensity and the balance of resultant white light emission based on large Stokes shift of the yellow monochromatic emitter. The incorporation of nano-sized POSS not only shows significant AIE effect, but also exhibits high thermal stability, which efficiently enhance the efficiency (Φ_{film}=95%) of the resultant hybrids (**W_{62}**) in solid state the deaggregation effect of POSS. This work provided a novel strategy for design and preparation of white-light-emitting molecules with high thermal stability, high emitting efficiency and well file formability.

Acknowledgement

This research was financially supported by the National Natural Science Fund of China (Grant Nos. 21671037, 21471030, 21271040).

View Article Online
DOI: 10.1039/C7NJ03692B

References

[1] M. R. Molla and S. Ghosh. *Chem. Eur. J*. 2012, **18**, 1290-1294.

[2] C. M. Zhong, C. H. Duan, F. Huang, H. B. Wu and Y. Cao. *Chem. Mater*., 2011, **23**, 326-340.

[3] Y. Zhang, C. A. Xie, H. P. Su, J. Liu, S. Pickering and Y.Q. Wang, J.A. Xu. *Nano. Lett*., 2011, **11**, 329-332.

[4] L. X. Xiao, Z. J. Chen, B. Qu, J. X. Luo, S. Kong, Q. H. Gong and J. J Kido. *Adv. Mater*., 2011, **23**, 926-952.

[5] S. Mukherjee, P. Thilagar. *Dyes. Pigm*., 2014, **110**, 2-27.

[6] A. Ozawa, A. Shimizu, R. Nishiyabu, Y. Kubo. *Chem. Commun*., 2015, **51**, 118-121.

[7] C. Chen, X. H. Jin, X. J. Zhou, L. X. Cai, Y. J. Zhang, J. Zhang *J. Mater. Chem. C*., 2015, **3**, 4563-4569.

[8] B. J. Xu, Y. X. Mu, H. Z. Wu and Y. Zhang. *Chem. Sci*., 2016, **7**, 2201-2206.

[9] V. R. K, K. K. R. Datta, and S. J. George. *Adv. Mater*., 2013, **25**, 1713-1718.

[10] P. Li, Q. Chen, J. Zhao, Z. Hu, D. Cao *J. Surfactant. Deterg*., 2011, **15**, 449-456.

[11] R. B. Wang, J. A. Peng, F. Qiu, Y. L. Yang *Chem. Commun*., 2009, **44**, 6723-6725.

[12] H. Sasabe, J. Takamatsu, G. Wagenblast and N. Langer, J. Kido. *Adv. Mater*., 2010, **22**, 5003-5007.

[13] S. K. Panda, S. G. Hickey, H. V. Demir and A. Eychmuller. *Angew. Chem. Int. Ed.,* 2011, **50**, 4432-4436.

[14] K. Kim, J. Y. Woo, S. Jeong and C. S. Han. *Adv. Mater*., 2011, **23**, 911-914.

[15] W. Mroz, C. Botta, U. Giovanella, E. Rossi and A. Colombo. *J. Mater. Chem*., 2011, **21**, 8653-8661.

[16] M. M. Zhang, S. C. Yin, J. Zhang and Z. X. Zhou, *PNAS*., 2017, **114**, 3044-3049.

[17] D. Chen, J. Y. Zhan, M. M. Zhang and S. C. Yin, *Polym. Chem*., 2015, **6**, 25-29.

[18] J. Liu, Y. Cheng, Z. Xie, Y. Geng, L. Wang, X. Jing and F. Wang. *Adv. Mater*., 2008, **20**, 1357-1362.

[19] J. Liu, L. Chen, S. Shao, Z. Xie, Y. Cheng, Y. Geng and F. Wang. *Adv. Mater*., 2007, **19**, 1859-1863.

[20] H. Wu., J. Zou, F. Liu, L. Wang and A. Mikhailovsky. *Adv. Mater*., 2008, **20**, 696-702.

View Article Online
DOI: 10.1039/C7NJ03692B

[21] L. Ying, C. Ho and H. Wu. *Adv. Mater*., 2014, **16**, 2459-2473.

[22] C. Gu, Y. Chen and Z. Zhang. *Adv. Energy. Mater*., 2014, **8**, 1289-1295.

[23] S. Park, J. E. Kwon, S. H. Kim, J. Seo and K. Chung. *J. Am. Chem. Soc*., 2009, **131**, 14043-14049.

[24] S. H. Kim, S. Park, J. E. Kwon and S. Y. Park. *Adv. Funct. Mater*., 2011, **21**, 644-651.

[25] X. H. Yang, J. D. Froehlich, H. S. Chae and S. Li. *Adv. Funct. Mater*., 2009, **19**, 2623-2629.

[26] K. Tanaka and Y. Chujo. *J. Mater. Chem*., 2012, **22**, 1733-1746.

[27] F. Wang, X. Lu, C. He. *J. Mater. Chem*., 2011, **21**, 2775-2782.

[28] Z. Yan, H. Xu, S. Guang, X. Zhao, W. Fan and X. Y. Liu. *Adv. Funct. Mater*., 2012, **22**, 345-352.

[29] B. H. Yang, H. Y. Xu, Z. Z. Yang, C. Zhang. *J. Mater. Chem*., 2010, **20**, 2469-2473.

[30] X. Y. Su, S. Y. Guang, C. W. Li and H. Y. Xu, *Macromolecules*, 2010, **43**, 2840-2845.

[31] B. H. Yang, H. Y. Xu, Z. Z. Yang and X. Y. Liu. *J. Mater. Chem*., 2009, **19**, 9038-9044.

[32] C. Zhang, S. Guang, X. Zhu, Xu H, X. Liu and M. Jiang. *J. Phys. Chem. C*., 2010, **114**, 22455-22461.

[33] X. Y. Su, S. Y. Guang, H. Y. Xu, X. Y. Liu, S. Li, X. Wang, P. Wang. *Macromolecules*, 2009, **42**, 8969-8976.

[34] Y. Feng, Y. Jia and H. Y. Xu. *J. Appl. Polym. Sci*., 2009, **111**, 2684-2690.

[35] Y. K. Zhu, S. Y. Guang, H. Y. Xu. *Chin. Chem. Lett.*, 2012, 1095-1098.

[34] Y. D. Xu, Q. Yang, Z. H. Shen, X. F. Chen, X. H. Fan and Q. F. Zhou. *Macromolecules,* 2009, **42**, 2542-2550.

[36] S. Sulaiman, A. Bhaskar, J. Zhang and R. Guda. *Chem. Mater*., 2008, **20**, 5563-5573.

[37] T. Stephan and K. Norbert. *J. Org. Chem*., 1998, **63**, 8551-8553.

[38] J. Wilbuer, D. C. Grenz, G. Schnakenburgc and B. Esser. *Org. Chem. Front*., 2017, **4**, 658-663.

[39] K. C. Tanja, T. Siham, W. Alexander and B. Martin. *Chem. Commun*., 2017, **53**, 1599-1602.

[40] Z. Z Li, F. Liang, M. P. Zhuo, Y. L and Shi, X. D. *Small*, 2017, **13**, 1604110-1604116.

[41] Z. Wang, B. Lin, X. Hu, C. Zhang. *ACS Appl. Mater. Inter*, 2017, **9**, 35253−35259

[42] B. Minaev, G. Baryshnikov and H. Agren. *Phys. Chem. Chem. Phys*., 2014, **16**, 1719-1758.

[43] U. Giovanella, C. Botta, F. Galeotti, B. Vercelli, S. Battiato and M. Pasini. *J. Mater. Chem. C*., 2013, **1**, 5322-5329.

[44] Y. K. Zhu, S. Y. Guang, H. Y. Xu, X. Y. Su and X. Y. Liu. *J. Mater. Res*., 2013, **8**, 1061-1069.

View Article Online
DOI: 10.1039/C7NJ03692B

[45] Y. K. Zhu, S. Y. Guang, X. Y. Su, H. Y. Xu, D. Y. Xu. *Dyes. Pigm*., 2013, **97**, 175-183.

[46] X. Y. Su, S, Y. Guang, H, Y. Xu, J, Y. Yang and Y. L. Song. *Dyes. Pigm*., 2010, **87**, 69-75.

[47] F. Y. Ke, C. Zhang, S. Y. Guang, H. Y. Xu and N. B. Lin. *J. Appl. Polym. Sci*., 2015, **132**, 42292.

[48] X. Wang, S. Y. Guang, H. Y. Xu, X. Y. Su and N. B. Lin. *J. Mater. Chem*., 2011, **21**, 12941-12948.

[49] S. Z. Wang, S. Y. Guang, H. Y. Xu and F. Y. Ke. *RSC Adv*., 2015, **5**, 1070-1078.

[50] F. Y. Ke, S. Z. Wang, S. Y. Guang, Q. Liu and H. Y. Xu. *Dyes. Pigm*., 2015, **121**, 199-203.

[51] X. Wang, S. Y. Guang, H. Y. Xu, X. Y. Su, J. Y. Yang, Y. L. Song and N. B. Lin. *J. Mater. Chem*., 2008, **18**, 4204-4209.

[52] C. Zhang, S. Y. Guang, X. B. Zhu, H. Y. Xu, X. Y. Liu and M. H. Jiang. *J. Phys. Chem. C*., 2010, **114**, 22455-22461.

[53] Y. K. Zhu, S. Y. Guang, H. Y. Xu, X. Y. Su and X. Y. Liu. *J. Mater. Chem. C*., 2013, **1**, 5277-5284.